Biomaterials Science

PAPER

View Article Online
View Journal

Cite this: DOI: 10.1039/d5bm01849h

Self-assembled biomimetic microenvironments with sulfated levan promote kidney epithelial cell growth and reduce inflammatory cytokine release

Dunya Arabi,[a] Annika Clemenz,[a] Cedric Wilden,[b] Paula Marie Schindler,[a] Julia Decker,[a] Nsrin Aroub,[a] Albrecht Berg,[c] Wolfgang Metzger,[d] Maike Derenek,[e] Samer Alokaidi,[f] Karin Jacobs,[f] Philipp Jung,[e] Matthias W. Laschke,[b] Emmanuel Ampofo[b] and Sandra Rother *[a]

Kidney diseases are a major global health burden, underscoring the need for new strategies to support renal repair. Biomimetic materials that recapitulate extracellular matrix functions can provide structural support while presenting biochemical cues that guide epithelial behavior. Here, we engineered self-assembled collagen type I microenvironments incorporating levan, sulfated levan (sLevan), pea starch (PEA), and sulfated PEA (sPEA) as a sustainable, non-animal-derived class of glycosaminoglycan (GAG) mimetics. Chemical sulfation of levan and starch introduced negative charge, enhanced solubility, and generated derivatives with moderate anti-factor Xa activity compared with heparin. Biochemical assays demonstrated that all polysaccharides were stably incorporated into collagen networks without hindering enzymatic degradability, while sulfation and polymer type modulated fibril assembly kinetics and coating morphology. In solution and when presented within collagen coatings, sPEA starch consistently reduced human kidney epithelial cell (HK-2) metabolic activity and cell numbers, indicating antiproliferative effects. In contrast, sLevan-containing microenvironments supported HK-2 proliferation under basal and hyperglycemic conditions comparable to heparin-containing controls. Notably, sLevan-functionalized coatings significantly suppressed secretion of the pro-inflammatory cytokine interleukin (IL)-6 and prevented glucose-induced increases in latent transforming growth factor (TGF)-β1, two mediators implicated in tubular inflammation and fibrotic remodeling. Together, these findings indicate that sulfation critically governs the bioactivity of levan- and starch-based GAG mimetics. Collagen/sLevan microenvironments combine tunable matrix assembly, moderate anticoagulant activity, and favorable epithelial growth and cytokine profiles under hyperglycemic stress, highlighting their potential as renewable GAG-mimetic platforms for renal tissue engineering and *in vitro* disease modeling.

Received 17th December 2025,
Accepted 16th May 2026

DOI: 10.1039/d5bm01849h

rsc.li/biomaterials-science

Introduction

Kidney diseases affect more than 850 million individuals worldwide and represent a leading cause of morbidity and mortality.[1–3] Disease progression is characterized by loss of renal function, ultimately leading to end-stage kidney disease, which requires renal replacement therapy (dialysis or transplantation). Kidney transplantation remains the most effective treatment for end-stage kidney disease, yet its application is severely constrained by a global shortage of donor organs and the need for life-long immunosuppression.[4] Consequently, there is a pressing need to develop alternative strategies for restoring or preserving kidney function.

In recent years, tissue engineering and regenerative medicine approaches have attracted increasing interest. Among these, cell-based therapies, engineered tissues, and biomimetic extracellular matrix (ECM) systems show promise for supporting kidney regeneration by promoting cell adhesion, survival, and specialized functions.[5–8] The ECM plays a central role in regulating tissue organization and function by providing both structural and biochemical cues.[9] In the context of kidney tissue engineering, the choice of scaffold materials is

[a]Institute of Biophysics, Center of Integrative Physiology and Molecular Medicine (CIPMM), Saarland University, 66421 Homburg, Germany.
E-mail: Sandra.rother@uks.eu
[b]Institute for Clinical and Experimental Surgery, Saarland University, PharmaScienceHub (PSH), 66421 Homburg, Germany
[c]Biomaterials Department, INNOVENT e.V., 07745 Jena, Germany
[d]Department of Trauma, Hand and Reconstructive Surgery, Saarland University, 66421 Homburg, Germany
[e]Institute of Medical Microbiology and Hygiene, Saarland University, 66421 Homburg, Germany
[f]Experimental Physics and Center for Biophysics, Saarland University, 66123 Saarbrücken, Germany

critical for recapitulating key features of the native ECM. Collagen type I, as the most abundant structural ECM protein in the kidneys, provides a fibrillar network that supports cell adhesion, spreading, and mechanotransduction.[10] However, collagen alone lacks certain biochemical cues present in the native renal microenvironment.[11] In line with this, kidney tissue engineering approaches have increasingly incorporated glycosaminoglycan (GAG)-containing matrices to better reproduce renal ECM complexity. For example, hyaluronan-based injectable hydrogels have been investigated for renal anti-inflammatory cytokine delivery after acute kidney injury, while kidney-derived decellularized ECM hydrogels retaining collagen and sulfated GAG components were shown to support renal cell viability and proliferation more effectively than collagen I alone.[12–14] However, these systems either rely on native tissue-derived ECM compositions or focus primarily on therapeutic delivery concepts rather than defined sulfated polysaccharide-mediated modulation of renal epithelial microenvironments. In this context, renewable, non-animal-derived sulfated polysaccharides represent an attractive yet still insufficiently explored strategy for engineering defined kidney-relevant collagen microenvironments.

GAGs, such as heparan sulfate, heparin (Hep) and chondroitin sulfate (CS) are linear polysaccharides that interact with growth factors, cytokines, and ECM proteins to modulate cell behavior, inflammatory responses, and tissue remodeling.[15,16] However, naturally derived GAGs are typically obtained from animal sources, raising concerns regarding variability, sustainability, and ethical acceptability.[17] These limitations have motivated the search for renewable and tunable GAG mimetics.[18] Incorporating GAG-mimetic polymers into collagen matrices offers the opportunity to combine the structural support of animal-derived collagen with the bioactive functionality of sulfated polysaccharides, potentially enhancing cell–matrix interactions.[19]

Levan, a β-(2 → 6)-linked fructan produced by bacteria, fungi, and plants, has emerged as a promising candidate. This branched, water-soluble polymer is biocompatible and biodegradable, with reported applications in food, pharmaceuticals, and cosmetics.[20] In addition, levan displays health-promoting effects, including prebiotic activity and immunomodulation.[21–24] Its chemical modification through sulfation yields sulfated levan (sLevan), which has previously been described as a biocompatible Hep-mimetic glycan with anticoagulant activity and has been explored in non-renal biomaterial formats, including bioactive thin films and adhesive multilayer membranes.[25,26] Such properties make levan and its derivatives attractive candidates for use as polysaccharide-based ECM mimetics in regenerative medicine.

In vitro fibrillogenesis of collagen I replicates the natural self-assembly process under physiological conditions, enabling the design of biomimetic scaffolds with tunable architectures.[27] Polysaccharides such as GAGs are known to influence this process, affecting fibril organization, and stability, thereby altering the biochemical and mechanical properties of the resulting matrix.[28,29] Inflammatory and profibrotic mediators strongly shape chronic kidney disease progression and are tightly regulated within the tubular microenvironment. Transforming growth factor (TGF)-β1 drives renal fibrosis and is produced by proximal tubule epithelial cells under injurious and hyperglycemic conditions, predominantly as a latent complex requiring local activation.[30] Interleukin (IL)-6 is a key mediator linking tubular injury, inflammation, and diabetic kidney disease, with elevated levels associated with adverse outcomes.[31]

Here, we investigate how levan, sLevan, and pea starch-based GAG mimetics tune the self-assembled collagen structures during fibrillogenesis to create customized biomimetic microenvironments. In addition, we assess the anticoagulant activity of sLevan and evaluate the effects of polysaccharide sulfation on proliferation, viability, and morphology of human kidney-2 (HK-2) cells under basal and hyperglycemic conditions. Furthermore, we quantify IL-6 and TGF-β1 secretion as readouts of inflammatory and profibrotic epithelial responses to the developed microenvironments. These analyses aim to provide mechanistic insight into polysaccharide/collagen interactions and to explore the potential of levan-based, non-animal GAG mimetics as growth substrates for kidney cells and *in vitro* disease modeling under high-glucose stress.

Materials and methods

Materials

Levan-H (Levan) was supplied by Real Biotech Co, Ltd, Chungnam, Korea. Pea starch (PEA) was provided by Emsland Group, Germany. Dimethylformamide (DMF), dimethylacetamide (DMAc) and SO_3/pyridine complex were purchased from Merck (Darmstadt, Germany). Acetone, sodium bicarbonate, sodium hydroxide and deuterium oxide (99.95 atomic % D) were supplied by Carl Roth GmbH + Co. KG (Karlsruhe, Germany). If not stated otherwise, chemical reagents were purchased from Merck, Darmstadt, Germany. Hep, derived from porcine intestinal mucosa, was purchased from Merck (Darmstadt, Germany), with a degree of sulfation of 2.2 per repeating disaccharide unit and an average molecular weight of 18 kDa. Levan with a molecular weight of 5 kDa was purchased from Innovent e.V. (Jena, Germany).

Synthesis of sulfated levan and sulfated pea starch

Sulfated polysaccharides were synthesized using a modified SO_3/pyridine method. As an example, levan was sulfated at a molar ratio of polymer to sulfating reagent of 1 : 20. For this purpose, 2 g (12 mmol) of levan was dissolved in dry DMF under an argon atmosphere. The SO_3/pyridine complex (39.26 g, 246.7 mmol) in 269 mL of dry DMF was added dropwise under continuous stirring. The reaction mixture was stirred at room temperature for one hour. Sulfation was quenched by the addition of distilled water (4.44 mL, 246.7 mmol), followed by stirring for an additional two minutes. The reaction mixture was precipitated into 3 L of acetone, and the resulting solid was collected using a slotted

nutsche filter and washed three times with acetone. The precipitate was dissolved in 100 mL of distilled water to yield a clear yellowish solution, which was adjusted to pH 7.5 with 10 N NaOH. The solution was then dialyzed (molecular weight cut-off 1 kDa) against 125 g of $NaHCO_3$ in 5 L of water for 4 days, followed by dialysis against distilled water. Final purification was achieved by drying under high vacuum using an oil pump. Typical yields were 75–80% (white solid). For sulfation of PEA starch, the same procedure was applied except that DMAc was used as solvent.

Chemical characterization of sulfated levan and sulfated pea starch derivatives

Fourier-transform infrared (FT-IR) spectra were acquired on an FT/IR-6800 spectrometer (Jasco GmbH, Pfungstadt, Germany) in the range of 4000–400 cm^{-1} using attenuated total reflection (ATR). Polymers containing fructose or glucose moieties exhibited characteristic IR bands. A broad and characteristic absorption band at 3200 cm^{-1} is due to the O–H stretching of rings and $-CH_2OH$ groups, while bands around 2850 cm^{-1} are due to the carbon–hydrogen (C–H) stretching vibrations of ring residues. In addition, absorption bands observed at 950, 1000 and 1100 cm^{-1} relate to the C–O–C symmetric bending vibration of rings and glycosidic linkages. Insertion of sulfate groups on the polysaccharide resulted in the formation of new bands. Bands at 1220 cm^{-1} were attributed to asymmetric vibrations of S–O associated with the distribution of sulfate groups on the molecule,[32,33] while the band at 808 cm^{-1} corresponds to symmetric vibrations of C–O–S of the $C–O–SO_3$ group.[34]

Nuclear magnetic resonance (NMR) spectroscopy was employed to confirm the introduction and distribution of sulfate groups along the polysaccharide backbone and to assign substitution sites on the fructose ring. NMR spectra were recorded in D_2O (99.9%, Sigma-Aldrich, Schnelldorf, Germany) with a Bruker Avance 400 MHz spectrometer at 373 K. Chemical shifts were referenced to residual D_2O at 4.75 ppm. For ^{13}C NMR, spectra were acquired on a Bruker DRX 400 NMR spectrometer in D_2O or in DMSO-d_6 at 70 °C overnight. Approximately 30 mg of polymer was dissolved in 700 μL of solvent. The reference signal of DMSO-d_6 was set at 2.49 ppm and D_2O at 4.75 ppm was used as a reference signal. The structural evidence was mainly based on the ^{13}C NMR spectrum of levan and sLevan, recorded in D_2O.

Molecular weight distributions were determined by gel permeation chromatography (GPC) using a Jasco PU-980 pump and Jasco RID-1531 refractive index detector. Separation was achieved with three Suprema-Gel columns (8 × 300 mm; pore sizes 100, 1000, and 30 000 Å; particle sizes 10–20 μm). Phosphate buffer (pH 7.4) was used as the mobile phase at 0.8 mL min^{-1}. Calibration was performed using pullulan standards (PSS, Mainz, Germany).

The average degree of substitution (DS) of sLevan and sPEA was determined by quantifying the sulfur content using an elemental analyzer (CHNS Eurovector EA3000, HEKAtech GmbH, Wegberg, Germany).

Preparation of self-assembled biomimetic microenvironments

Each polysaccharide (Levan, sLevan, PEA, sPEA or Hep) was first dissolved in an equal volume of fibrillogenesis buffer (50.15 mM Na_2HPO_4, 11.17 mM KH_2PO_4, pH 7.4). In parallel, rat tail collagen type I (Corning, USA) was diluted in chilled 10 mM acetic acid to a final concentration of 1 mg mL^{-1}. The collagen solution was then mixed on ice with either the fibrillogenesis buffer alone or with buffer containing the respective polysaccharide, resulting in a final collagen concentration of 0.5 mg mL^{-1}. Unless otherwise stated, the collagen-to-polysaccharide mass ratio was 5 : 1 in all formulations according to previously published protocols with native GAGs.[35] The mixtures were incubated overnight at 37 °C in microwell plates for *in vitro* fibrillogenesis, forming a thin hydrogel layer. The microenvironments were dried under sterile conditions at room temperature, washed twice with sterile water and dried again, yielding thin coating-like films. Collagen-based microenvironments without polysaccharides (Coll) served as control. The generated polysaccharide-containing microenvironments were designated according to the incorporated polysaccharide type as Coll/Levan, Coll/sLevan, Coll/PEA, Coll/sPEA and Coll/Hep.

Biochemical characterization of self-assembled biomimetic materials

The stability of the prepared materials was evaluated by incubating the functionalized microenvironments with phosphate-buffered saline (PBS) at 37 °C for up to 14 days. At each time point, supernatants were collected for analysis and replaced with fresh PBS solutions. The sLevan and sPEA starch contents bound to collagen were quantified using the 1,9-dimethylmethylene blue (DMMB) assay after treatment with papain at 60 °C for 24 hours prior to analysis, as described previously for GAG-containing collagen coatings.[36,37] The bicinchoninic acid (BCA) assay was performed according to the manufacturer's instructions (Thermo Fisher Scientific, Dreieich, Germany) to determine the concentration of unbound collagen in the supernatant. Collagen type I was used to generate the standard calibration curve.

A starch colorimetric/fluorometric assay kit (Merck, Darmstadt, Germany) was used according to the manufacturer's protocol to quantify the release of PEA starch from the materials. In brief, 20 μL of the supernatant was mixed with 180 μL of hydrolysis buffer. From this mixture, 50 μL was transferred into each well of a 96-well plate. The standard solution was prepared accordingly. Then, 2 μL of hydrolysis enzyme mix was added to each sample and standard well, followed by incubation at room temperature for 30 minutes to allow hydrolysis. For color development, a reaction mixture was prepared and added at a volume of 50 μL per well. Finally, the absorbance was measured at 535 nm using a plate reader (Infinite M200Pro, Tecan, Crailsheim, Germany).

A total carbohydrate assay kit was used to determine levan in the supernatants following the manufacturer's protocol (Merck, Darmstadt, Germany). In brief, 150 μL of concentrated sulfuric acid was added to 30 μL of sample solution. The samples were incubated at 90 °C for 15 minutes. After incu-

bation, 30 μL of developer solution was added to each tube, and the mixture was shaken for 5 minutes at room temperature. Samples and standards were then transferred to a 96-well plate, and the absorbance was measured at 490 nm using a plate reader (Infinite M200Pro, Tecan, Crailsheim, Germany).

Coating integrity after 5 days of incubation (37 °C, 2% BSA/PBS) was assessed qualitatively by Sirius Red staining for collagen and Toluidine Blue staining for sulfated GAGs as described previously.[38] For Toluidine Blue staining, samples were incubated in 0.4 mg ml^{-1} Toluidine Blue in 0.1 M HCl containing 2 mg ml^{-1} NaCl for 4 hours at room temperature under shaking conditions and subsequently washed with water. For Sirius Red staining, samples were incubated in 0.1% Sirius Red in picric acid for 1 hour and washed with 0.01 M HCl to remove unbound dye. Stained coatings within the well plates were scanned using an Epson Perfection V850 Pro flatbed scanner and visually evaluated.

Enzymatic degradation of self-assembled biomimetic materials

The prepared materials were pre-incubated in PBS at 37 °C for one hour. Subsequently, a collagenase solution (1 mg mL^{-1} in PBS; 576 U mL^{-1}) was added to each sample. Materials treated with PBS alone (without collagenase) served as controls without degradation. At designated time points, the enzymatic reaction was terminated by removing the collagenase solution and immediately adding 0.2 M ethylenediaminetetraacetic acid (EDTA, Thermo Fisher Scientific, Dreieich, Germany) to inhibit further matrix degradation. Following each incubation, wells were aspirated and stained with Sirius Red for 15 minutes to visualize the remaining ECM. Excess stain was removed, and wells were washed three times with 0.01 M HCl. Plates were imaged, and subsequently, matrix-bound Sirius Red was eluted using 0.1 M NaOH. The eluates were transferred to a 96-well plate, and absorbance was recorded at 540 nm using a microplate reader (Infinite M200Pro, Tecan, Crailsheim, Germany).

Atomic force microscopy (AFM)

For AFM analysis, the coatings were prepared in 8 mm spacers positioned in the center of glass-bottom FluoroDishes (World Precision Instruments, Friedberg, Germany). AFM measurements were performed using a NanoWizard 4XP AFM system (JPK Instruments/Bruker, Germany) in PBS under hydrated conditions. Samples were analyzed using FastScan-D cantilevers (Bruker) in PeakForce Tapping mode. The applied force setpoint ranged between 0.3 and 0.6 nN. Height images were recorded and processed using a high-pass filter to enhance visualization of surface-associated structural features and local topographical organization.

Kinetic analysis of the self-assembling of microenvironments

Collagen solutions (0.5 mg mL^{-1}) dissolved in 10 mM acetic acid were mixed with different concentrations of polysaccharide solutions dissolved in 60 mM phosphate buffer (pH 7.4) at 37 °C in pre-warmed transparent 96-well plates. The kinetics of collagen monomer self-assembly in the presence of the polymers was analyzed over time by measuring the increase of turbidity at 313 nm, as described previously.[28,39] For each sample, measurements were performed in triplicate. The resulting turbidity curves were analyzed using GraphPad Prism 10. Raw data were first baseline-corrected by subtracting the mean of the initial five time points. The curves were then fitted individually for each replicate using a Gompertz growth model. From the fitted curves, the following kinetic parameters were extracted: maximal turbidity (A_{max}, corresponding to the asymptotic plateau), half-time of fibrillogenesis ($t_{1/2}$, corresponding to the inflection point), lag time (t_{lag}, calculated as $t_{1/2}$ minus the reciprocal of the growth rate, $1/K$), and growth time (t_g, calculated as $1/K$). Mean values and standard deviations were calculated across replicates for each experimental condition.

Anti-factor Xa activity assay

Anti-factor Xa activity was measured using the Biophen Heparin Anti-Xa assay (Hyphen BioMed) adapted to a 96-well microplate format. Each reaction contained 30 μL of sample, 30 μL of human antithrombin, 30 μL of factor Xa, 30 μL of chromogenic substrate and 50 μL of 2% citric acid at the end. Assays were performed in 25 mM HEPES buffer, pH 7.4, supplemented with 150 mM NaCl. The resulting absorbance was measured at 405 nm using a microplate reader (Infinite M200Pro, Tecan, Crailsheim, Germany). Residual anti-factor Xa activity was normalized to the activity in the absence of polysaccharide (set to 100%). Dose–response data were fitted with a four-parameter logistic model, and IC_{50} values were calculated using GraphPad Prism 10.

Chondroitin sulfate degradation assay

To analyze the impact of levan and PEA starch derivatives on the enzymatic degradation of the native GAG CS, an enzyme-linked immunosorbent assay (ELISA) was employed. CS (from pig, degree of sulfation 0.8, 19.8 kDa) was first dissolved in 25 mM citrate-phosphate buffer to a final concentration of 1 mg mL^{-1}. Then, CS chains were covalently immobilized onto MaxiSorp 96-well microtiter plates (Thermo Fisher Scientific, Schwerte, Germany) *via* their reducing ends, following the method described previously.[40,41] To block non-specific binding, uncoated wells were incubated with 1% (w/v) bovine serum albumin (BSA) in Tris-buffered saline (TBS). CS degradation was analyzed using chondroitinase ABC (ChABC; Sigma, C2905-10UN-PW). Test samples of 100 μg mL^{-1} levan, sLevan, PEA starch and sPEA starch, controls, and references were prepared in buffer (50 mM Tris, 150 mM NaCl, pH 7.9) with or without 5 mU ChABC per well. CS-coated 96-well plates were pre-incubated with PBS at 37 °C for one hour. After removal of PBS, prewarmed samples and enzyme solutions were added and incubated for one hour at 37 °C. Plates were washed three times with PBS containing 0.05% Tween-20. Residual CS was detected using mouse anti-CS monoclonal antibody (clone CS-56; Sigma, C8035, 1 : 1250 in 1% BSA/PBS, 30 minutes), followed by horse radish peroxidase (HRP)-conjugated goat anti-mouse IgG addition (Invitrogen, 31 430;

1 : 10 000 in 1% BSA/PBS, 30 minutes, in the dark). After final washing, substrate solution was added, and color development was stopped with 2 N H_2SO_4. Absorbance was measured at 450 nm with 570 nm as reference using a microplate reader (Infinite M200Pro, Tecan, Crailsheim, Germany).

Protein binding to the self-assembled biomimetic materials

Rhodamine B-labeled lysozyme (Nanocs Inc., New York, NY, USA) was used as a model protein to investigate its interaction with self-assembled biomimetic material surfaces. Microenvironments were prepared in 48-well plates and incubated with 500 μL of lysozyme solution (30 μg mL^{-1} in 2% BSA/PBS) at 4 °C overnight. After incubation, the supernatant was collected and the fluorescence intensity was measured to determine the amount of unbound lysozyme. Fluorescence measurements were performed at an excitation wavelength of 544 nm and an emission wavelength of 576 nm. ECM samples incubated with 2% BSA in PBS without lysozyme served as blanks and were used for background correction. Protein binding to the ECM was quantified by comparing the fluorescence intensity of the supernatant after incubation to that of the initial lysozyme solution.

Cell culture of HK-2 cells

HK-2-cells were kindly provided by Prof. Leticia Prates Roma (Saarland University, Germany). HK-2 cells were cultivated in keratinocyte serum-free-medium (Keratinocyte SFM, Gibco, Life Technologies GmbH, Darmstadt, Germany) supplemented with keratinocyte growth supplement kit and 1% penicillin–streptomycin (10 000 U mL^{-1}) (Gibco, Thermo Fisher Scientific, Darmstadt, Germany) at 37 °C and 5% CO_2.

To evaluate the effects of soluble polysaccharides on cell proliferation and viability, 10 000 cells were seeded in 96-well plates and treated with varying concentrations of the respective polysaccharides under basal or high glucose (30 mM glucose) conditions for 72 hours. After treatment, cell viability was measured. For cell quantification, samples were washed with PBS and stored at −80 °C until further analysis.

In addition, 10 000 HK-2 cells were seeded onto the developed microenvironments in 96-well plates in the presence or absence of glucose supplementation. Tissue culture polystyrene (TCPS) was included as additional reference. The cells were cultivated for 48 hours prior to further measurements. To distinguish glucose-specific from osmotic effects, cells were additionally cultured accordingly on Coll and Coll/sLevan coatings in the presence of 30 mM mannitol as an osmotic control. For this analysis, IL-6 secretion was quantified by ELISA after 48 hours.

For analysis of cell morphology, 10 000 cells were seeded into 8-well chamber slides (Thermo Fisher Scientific, Darmstadt, Germany) and treated with 50 μg mL^{-1} of levan, sLevan, PEA starch and sPEA starch for 72 hours.

Quantification of cell viability

Cell viability was quantified using the Celltiter-Blue Cell Viability Assay (Promega Corporation, Germany). After HK-2 treatment with polysaccharides or culture on biomimetic materials, 30 μL of the Celltiter-Blue reagent was applied to each well and incubated for 2–4 hours at 37 °C under 5% CO_2. Fluorescence intensity was detected using a microplate reader Infinite M200Pro (Tecan, Crailsheim, Germany) with λ_{ex} = 560 nm, and λ_{em} = 590 nm. Each material type was tested with a sample size of n = 8 per condition.

Quantification of cell numbers

DNA content in cell lysates was determined using the Quant-iT PicoGreen dsDNA assay reagent (Thermo Fisher Scientific, Darmstadt, Germany). Cells were thawed on ice for 10 minutes and lysed by incubation with 1% Triton X-100 in PBS on ice for 1 hour. Subsequently, 10 μL of the lysate was mixed with 190 μL of PicoGreen dsDNA reagent (1 : 800 dilution in Tris-EDTA buffer (10 mM Tris base, 1 mM EDTA)) in a black 96-well plate. The mixture was incubated for 5–10 minutes at room temperature in the dark. Fluorescence intensity was measured using a microplate reader (Infinite M200Pro, Tecan, Crailsheim, Germany) with settings of λ_{ex} = 485 nm and λ_{em} = 535 nm. Each material type was tested with a sample size of n = 5 per condition. DNA quantification was calibrated using λ-DNA (Thermo Fisher Scientific, Darmstadt, Germany). To relate DNA content to cell number, a calibration curve based on defined HK-2 cell numbers was applied, enabling calculation of DNA per cell.

Immunofluorescence staining and microscopy

Cells were fixed in 4% paraformaldehyde (PFA) for 10 minutes and washed three times with PBS. For long-term storage at 4 °C, 90% of the solution was replaced by PBS. Cell permeabilization was achieved by incubation with 0.1% Triton X-100 in PBS for 20 minutes, followed by washing with PBS. To block non-specific binding, cells were incubated with 1% BSA in 0.05% Tween20 in PBS for 10 minutes. AlexaFluor-568 phalloidin (1 : 200 dilution, Thermo Fisher Scientific (Darmstadt, Germany)) was applied for 60 minutes protected from light. Afterwards, cells were washed three times with PBS. To prepare the samples for imaging, cells were mounted using Fluormount-G containing DAPI (4′,6-diamidino-2-phenylindole) from Thermo Fisher Scientific (Darmstadt, Germany) and allowed to dry overnight at room temperature. After drying, the samples were stored at 4 °C. Fluorescence microscopy (Olympus, Germany) was used to visualize cell morphology, with detection filters set to λ_{em} = 578 nm for AlexaFluor-568 and λ_{ex} = 365 nm and λ_{em} = 420 nm for DAPI.

IL-6 and TGF-β1 quantification *via* enzyme-linked sorbent assays (ELISA)

Supernatants were collected after HK-2 cultivation on the biomimetic materials for 48 hours and stored at −20 °C until analysis. IL-6, and active and latent TGF-β1 concentrations were quantified using the human IL-6 and human TGF-β1 DuoSet ELISA (R&D Systems GmbH, Wiesbaden-Nordenstadt, Germany). The assays were performed according to the manufacturer's protocols. Each material type was tested with a sample size of n = 4.

Interaction of IL-6 with polysaccharides

Hep and the sulfated GAG mimetics sPEA starch and sLevan were covalently immobilized onto 96-well ELISA plates as described previously.[41] BSA-coated wells served as controls for non-specific binding. The polysaccharide-coated plates were incubated with 5, 25 or 50 nM IL-6 dissolved in PBS with 1% BSA for 16 hours at 4 °C. Afterwards, the supernatants were collected, and the amount of non-bound IL-6 was quantified by ELISA as described above. Each condition and concentration was tested with a sample size of $n = 3$.

Statistical analysis

Statistical analyses were performed using GraphPad Prism version 10.6.1 (GraphPad Software, San Diego, CA, USA). Unless otherwise stated, data are presented as mean ± standard deviation (SD). Comparisons between multiple groups were conducted using one-way analysis of variance (ANOVA) followed by Tukey's multiple-comparisons test. For experiments involving two independent variables, two-way ANOVA followed by Dunnett's multiple-comparisons test was applied. Statistical significance was defined as $p < 0.05$.

Results

Preparation of sulfated levan and PEA starch derivatives

Chemical sulfation of the natural polysaccharides levan and PEA starch was performed to obtain the corresponding sulfated GAG mimetics (Fig. 1). Structural modifications were confirmed by NMR spectroscopy for levan. Comparison of the ^{13}C NMR spectra of native levan and sLevan revealed characteristic low-field shifts consistent with sulfate substitution (Table 1). The C1 signal of the primary CH_2 group in the fructose unit shifted from 61 to 63 ppm upon sulfation. Additional downfield shifts and signal splitting at C3 and C4 demonstrated partial substitution at these hydroxyl groups. The C1 position was preferentially sulfated with subsequent sulfate substitution occurring on C3 and C4 without preference, resulting in a derivative that was fully sulfated at C1 and partially sulfated at C3 and C4. The C5 signal was also broadened in the presence of a sulfated environment. For C2 and C6, the linkage carbons, the signals shifted upfield from 104 to 102 ppm and downfield from 63 to 66 ppm, respectively, as expected when the molecule is substituted with a negative group. Analytical data for all synthesized derivatives are summarized in Table 2. Both sLevan and sPEA were obtained as water-soluble white solids. For sPEA starch, sulfation was confirmed by IR spectroscopy and elemental analysis. Due to the high molar mass ($M_w = 1.84 \times 10^6$ g mol^{-1}), NMR spectra could not be evaluated.

Composition and stability of self-assembled biomimetic microenvironments

Self-assembled biomimetic materials containing levan and PEA starch (Coll/Levan, Coll/PEA) as well as their sulfated derivatives (Coll/sLevan, Coll/sPEA) were prepared by incorporation of these polysaccharides during *in vitro* fibrillogenesis of collagen (Fig. 2A). Matrices with the native GAG Hep served as control (Coll/Hep). Collagen and polysaccharide stability of the

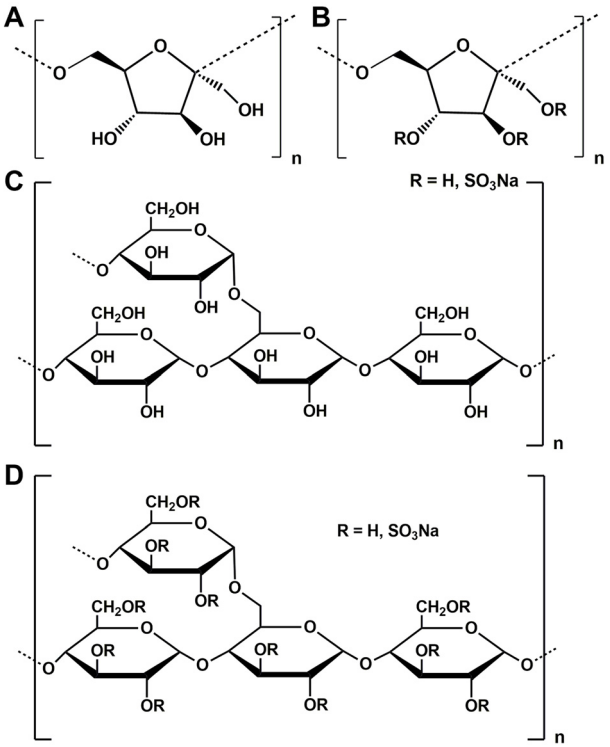

Fig. 1 Chemical structures of levan (A), starch (C) and their sulfated derivatives (B and D).

Table 1 Assignments of ^{13}C NMR spectra of unmodified and sulfated levan (400 MHz; in D_2O, chemical shifts in ppm)

Position	Levan	sLevan
C1	61.25	63.50
C2	104.87	102.88; 102.60
C3	76.88	79.38; 79.27
C4	75.57	76.01; 75.26
C5	80.41	81.05; 80.93
C6	63.12	66.50; 65.71

Table 2 Characteristic parameters of sulfated levan and pea starch derivatives

Sample	Levan	PEA starch	sLevan	sPEA starch
Sulfur content (%)	0	0	15.80	14.10
DS	0	0	1.52	1.30
M_n (g mol^{-1})	455 105	n.d.	18 588	4.95×10^5
M_w (g mol^{-1})	1 080 000	n.d.	27 332	1.84×10^6
PD	2.37	n.d.	1.47	3.73

Degree of sulfation (DS), and number-average (M_n) and weight-average (M_w) molecular weights were determined by RI detection. Molecular weight distributions (polydispersity index: PD) are based on the values calculated from RI detection; n.d.: not determined (compound is not soluble in the GPC eluent).

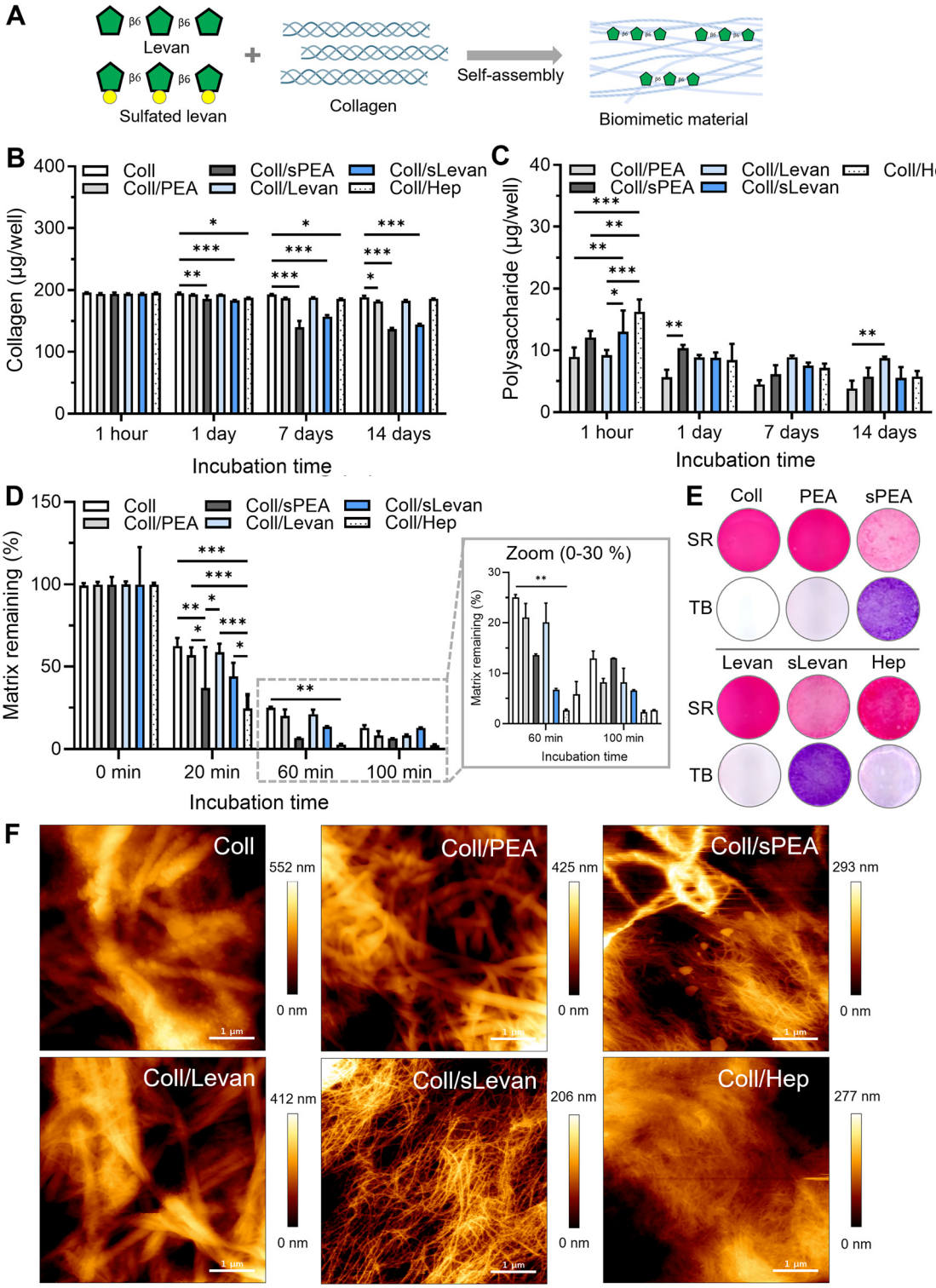

Fig. 2 Preparation and characterization of self-assembled biomimetic materials. (A) Schematic representation of the self-assembly process of biomimetic materials containing sulfated levan during *in vitro* collagen fibrillogenesis. (B) Collagen stability was assessed by BCA assay. (C) Polysaccharide incorporation was quantified using photometric assays. (D) Enzymatic degradation of the materials *in vitro* was evaluated by Sirius Red staining of the remaining matrix following collagenase treatment at 37 °C. Statistical analysis was performed using two-way ANOVA: * $p < 0.05$, ** $p < 0.01$, *** $p < 0.001$. Significant differences compared to collagen-only controls (Coll) are indicated for B. (E) Coating integrity after 5 days (37 °C, 2% BSA/PBS) assessed by Sirius Red (SR, upper panel for collagen) and Toluidine Blue (TB, lower panel for sulfated GAGs) staining. (F) Representative AFM height images of self-assembled collagen-based materials containing the respective polysaccharides (PEA, sPEA, levan, sLevan, Hep) compared with pure collagen under hydrated conditions in PBS. Scale bar = 1 µm.

self-assembled materials was monitored over time at 37 °C (Fig. 2B and C). Pure collagen coatings remained largely stable regarding their collagen content, showing only a 5–6% decrease after 14 days compared to the initial value (Fig. 2B). Coll/PEA, Coll/Levan, and Coll/Hep exhibited similar stability, with collagen loss of about 5–7% over the incubation period. In contrast, Coll/sPEA and Coll/sLevan showed an increased collagen release. For Coll/sPEA, collagen content was reduced by about 28–30% after 7 days relative to the starting value. The collagen content in the Coll/sLevan coatings also decreased steadily, reaching about 25% loss after 14 days.

Regarding the polysaccharide incorporation into the materials (Fig. 2C), Coll/sPEA and Coll/sLevan showed initial values in the range of 11–13 μg per well and a continuous decrease over time, with a 50–60% reduction after 14 days. Coll/PEA started at comparable levels (8–10 μg per well) and declined steadily to about 60% of the initial value. Coll/Levan exhibited relatively stable values between 8 and 10 μg per well throughout the experiment, with only minor changes. Coll/Hep showed the highest initial values (15–18 μg per well) but decreased strongly within one day (40–60% loss), followed by a more gradual decline up to 14 days.

The enzymatic degradation of the self-assembled materials by collagenase was analyzed *in vitro* (Fig. 2D). Coll retained 60–68% of its initial matrix after 20 minutes, 24–25% after 60 minutes, and 11–14% after 100 min. Coll/Levan and Coll/sLevan showed comparable degradation profiles. Coll/Hep degraded rapidly, leaving less than 3% after 60 minutes. After 100 minutes, no significant differences were observed between the groups. Coating integrity after 5 days of incubation (37 °C, 2% BSA/PBS) was assessed by Sirius Red and Toluidine Blue staining (Fig. 2E), confirming the presence of collagen and sulfated GAG mimetics in the respective coatings.

AFM demonstrated a polysaccharide type-dependent matrix morphology (Fig. 2F). For Coll, Coll/PEA starch and Coll/Levan, typical fibrillar collagen structures were observed. In contrast, Coll/sPEA starch materials displayed an altered structure with smaller collagen fibers. Coll/sLevan samples presented a dense and homogeneous fibrillar network. Coll/Hep exhibited a more diffuse and less distinct fibrillar organization compared to pure collagen. Overall, Coll/sLevan, Coll/Hep, and Coll/sPEA showed lower maximum height variations than Coll, Coll/PEA, and Coll/Levan.

Influence of GAG mimetics on collagen self-assembly

The influence of the synthesized GAG mimetics on collagen self-assembly was further assessed by monitoring turbidity for different collagen-to-polysaccharide ratios (Fig. 3 and Table 3). Pure collagen exhibited typical fibrillogenesis kinetics, with a lag time of 217 ± 14 s, a growth time of 106 ± 3 s, maximal turbidity of 0.290 ± 0.025, and $t_{1/2}$ of 323 ± 17 s. The presence of GAG mimetics modulated these parameters in a concentration-

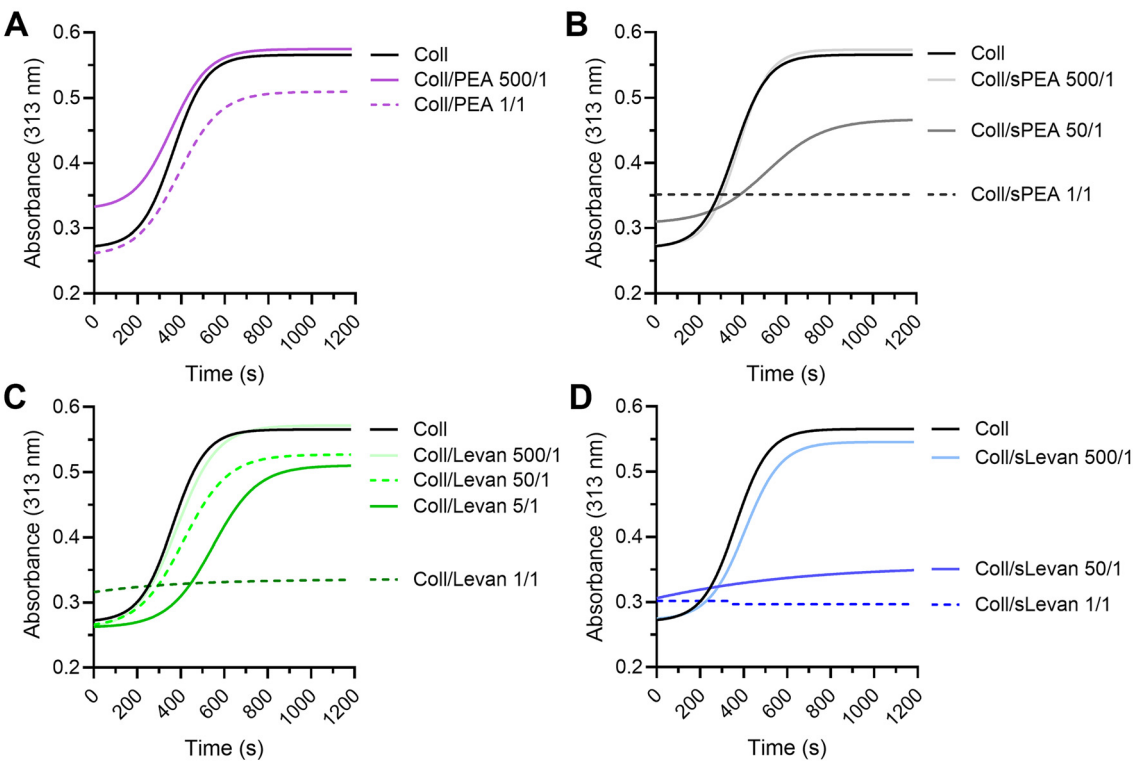

Fig. 3 Kinetics of microenvironment self-assembly. The *in vitro* fibrillogenesis of collagen type I was monitored by turbidity measurements at 313 nm in the presence of various collagen-to-polysaccharide mass ratios (1/1 to 500/1). The following polysaccharides were examined: PEA starch (A), sPEA starch (B), levan (C) and sLevan (D) in 60 mM phosphate buffer. Each curve represents the mean of three independent measurements.

Table 3 Influence of polysaccharides on kinetics of microenvironment self-assembly. The lag time (t_{lag}), growth time (t_g), maximal turbidity (A_{max}) and $t_{1/2}$ were calculated from the turbidity measurements at 313 nm after baseline correction in the presence of various collagen-to-polysaccharide mass ratios; ■: no sigmoidal fibrillogenesis curves were obtained

Parameter	t_{lag} (s)	t_g (s)	Turbidity (A_{max})	$t_{1/2}$ (s)
Coll	217 ± 14	106 ± 3	0.290 ± 0.025	323 ± 17
Coll/PEA 1/1	208	114 ± 27	0.278	317
Coll/PEA 500/1	159 ± 48	104 ± 5	0.233 ± 0.007	299 ± 48
Coll/sPEA 1/1	■	■	■	■
Coll/sPEA 50/1	243 ± 42	219 ± 45	0.171 ± 0.016	438 ± 6
Coll/sPEA 500/1	234.3	101 ± 8	0.334	344
Coll/Levan 1/1	■	■	■	■
Coll/Levan 500/1	224 ± 36	114 ± 40	0.311 ± 0.066	350 ± 84
Coll/sLevan 1/1	■	■	■	■
Coll/sLevan 50/1	■	■	■	■
Coll/sLevan 500/1	246 ± 21	117 ± 15	0.274 ± 0.026	368 ± 38

and type-dependent manner. Levan completely inhibited detectable fibrillogenesis at a 1 : 1 collagen-to-polysaccharide ratio, while at 500 : 1, normal fibril formation was observed, showing kinetics like collagen alone. Similarly, sLevan altered fibrillogenesis at lower ratios (1 : 1 and 50 : 1), but at a high dilution (500 : 1) the self-assembly resumed with slightly prolonged t_{lag} and $t_{1/2}$ compared to collagen. In contrast, low-molecular weight levan (5 kDa) did not reproduce the altered fibrillogenesis kinetics (SI Fig. S1). For PEA starch, fibrillogenesis was largely unaffected at 1 : 1 ratios and was slightly accelerated at 500 : 1. In contrast, sPEA starch inhibited fibril formation at 1 : 1, while intermediate and high dilutions (50 : 1 and 500 : 1) allowed self-assembly, although the growth time and $t_{1/2}$ were markedly altered at 50 : 1, indicating slower kinetics.

Effects of polysaccharide sulfation on anti-factor Xa activity and GAG breakdown

To assess the functional relevance of polysaccharide sulfation, anti-factor Xa activity and enzymatic degradation assays were performed to evaluate Hep-like anticoagulant properties and potential effects on the enzymatic degradation of GAGs. Sulfation of PEA starch and levan confers anticoagulant activity, as shown by dose-dependent inhibition of factor Xa (Fig. 4A and Table 4). Hep exhibited the highest potency with an IC_{50} of 0.26 μg mL^{-1}, whereas sLevan and sPEA starch were less active, showing IC_{50} values of 5.0 and 6.4 μg mL^{-1}, respectively. This corresponds to an approximately 19-fold (sLevan) and 24-fold (sPEA) lower inhibitory potency compared to Hep. In addition, the influence of sPEA starch, sLevan and Hep on the enzymatic degradation of the native GAG CS was evaluated (Fig. 4B). Here, no significant differences in the amount of enzymatically removed CS was detected in the presence of GAG mimetics or Hep.

Impact of different GAG mimetics on renal epithelial cell viability and growth

As proximal tubule epithelial cells are key responders to inflammatory and metabolic stress in the kidneys, we next evaluated how soluble GAG mimetics affect metabolic activity and cell numbers of HK-2 cells (Fig. 5). Treatment of HK-2 cells with different soluble polysaccharides for 72 hours led to distinct effects on metabolic activity and cell number under both basal and high glucose conditions (Fig. 5A–D). For metabolic activity, PEA starch reduced activity by about 30–50% compared to the polysaccharide-free control (Ctrl) across all concentrations. sPEA starch exerted even stronger inhibition at 10 μg mL^{-1} (40–60% less than Ctrl), with only partial recovery at higher concentrations (50–500 μg mL^{-1}, 20–40% less than Ctrl). Levan displayed mostly no significant effects on meta-

Table 4 IC_{50} values of sulfated polysaccharides determined for anti-factor Xa activity

Polysaccharide	Hep	sLevan	sPEA
IC_{50} (μg mL^{-1})	0.26 ± 0.11	4.98 ± 1.27	6.39 ± 0.26

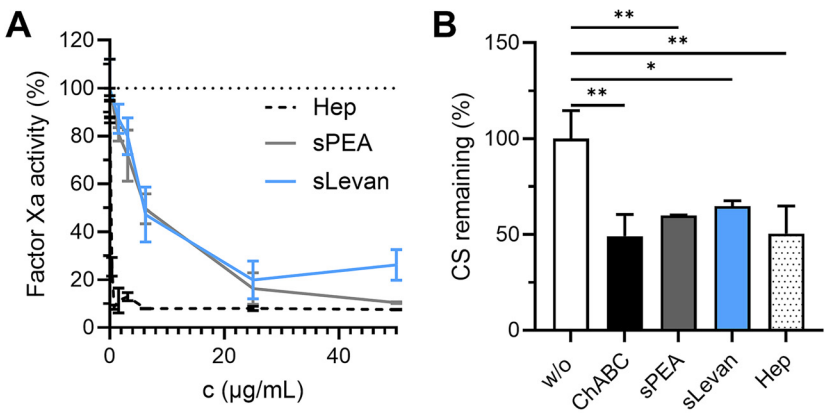

Fig. 4 Anticoagulant activity of sulfated levan and PEA starch derivatives and the effects on enzymatic CS degradation. (A) Anti-factor Xa activity of sulfated levan (sLevan) and sulfated PEA starch (sPEA starch) was determined in comparison with Hep using a chromogenic assay. (B) CS degradation by ChABC in the presence or absence of 100 μg mL^{-1} sPEA starch, sLevan, or Hep was quantified by ELISA with the CS-56 antibody. One-way ANOVA: * $p < 0.05$ ** $p < 0.01$.

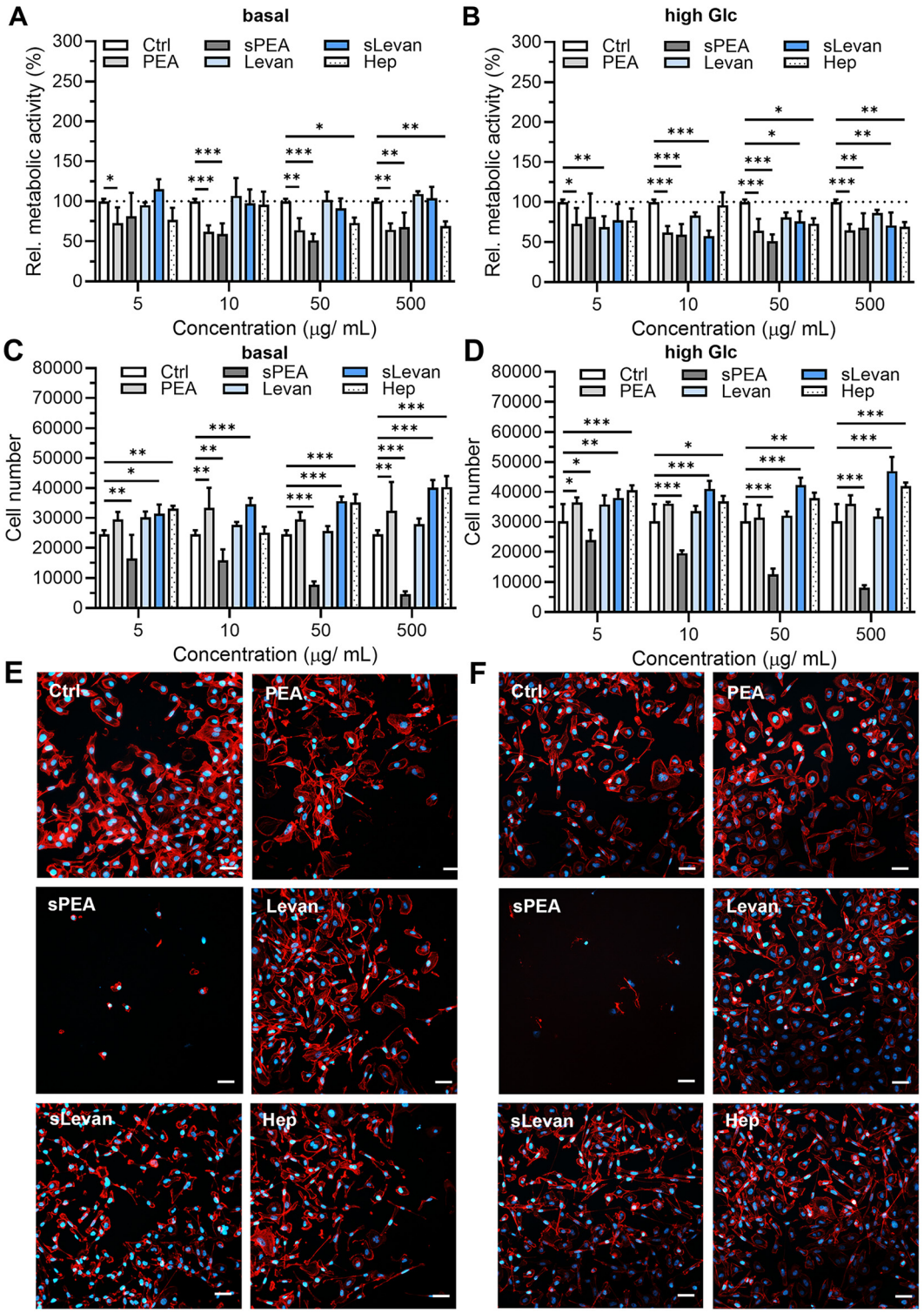

Fig. 5 Effects of soluble polysaccharides on HK-2 cell metabolic activity, cell number and morphology. The metabolic activity relative to Ctrl (A and B) and DNA amount (C and D) were quantified after 72 hours of HK-2 cell treatment with PEA, sPEA, levan, sLevan and Hep under basal or high glucose conditions relative to untreated cells in basal media (dotted line). Two-way ANOVA: * $p < 0.05$, ** $p < 0.01$, *** $p < 0.001$. Significant differences compared to Ctrl cells without treatment are shown. (E and F) Cells were stained for their cytoskeleton (AlexaFluor-568 phalloidin, red) and nuclei (DAPI, blue) after 72 hour treatment with 50 μg mL^{-1} polysaccharide solution under basal (E) or high glucose (F) conditions. Scale bars represent 50 μm.

bolic activity. sLevan induced no significant changes compared to untreated Ctrls under basal conditions. However, all tested sLevan concentrations above 5 μg mL^{-1} significantly reduced the metabolic activity under high glucose conditions. Hep showed variable responses, maintaining near-control levels at low doses but significantly reducing activity at 50–500 μg mL^{-1} (about 0.7–0.8-fold).

For DNA content, PEA starch and levan had no significant impact on the cell numbers independently on the cultivation conditions (Fig. 5C and D). sPEA starch significantly reduced DNA content in a dose-dependent manner, falling to about 0.2–0.4-fold of Ctrl at 50–500 μg mL^{-1}. In contrast, sLevan significantly promoted cell proliferation under high glucose conditions, reaching about 1.5–1.8-fold of Ctrl across all concentrations (Fig. 5D). Hep treatment also enhanced DNA content under hyperglycemic conditions, with increases of about 1.3–1.7-fold compared to Ctrl, especially at higher concentrations. Of note, calculated DNA per cell values were within the expected range for mammalian cells (SI Fig. S2A).

Morphological staining supported the quantitative findings (Fig. 5E). sPEA starch-treated HK-2 cells displayed reduced density and altered cytoskeletal structure, whereas sLevan- and Hep-treated cells retained normal morphology with preserved actin organization.

Sulfated levan-containing microenvironments promote renal epithelial cell proliferation

To assess how different collagen-based microenvironments influence HK-2 function and cell growth, both metabolic activity and cell number were measured (Fig. 6). Under basal conditions, the metabolic activity of HK-2 cells on Coll/PEA and Coll/Levan were comparable to Coll (Fig. 6A). Cells on Coll/sPEA showed significantly reduced activity (50–60% less than on Coll). Cells on Coll/sLevan and Coll/Hep showed metabolic activities comparable to cells on Coll and TCPS. Under high glucose conditions, the metabolic activity of HK-2 cells on Coll/PEA and Coll/Levan remained close to values on Coll and TCPS (Fig. 6B). The metabolic activity on Coll/sPEA remained significantly reduced compared to Coll as seen under basal conditions. No significant differences between cell metabolic activity on Coll or Coll/Hep were detected. In contrast, the metabolic activity of HK-2 cells on Coll/sLevan was lower than on TCPS, Coll or Coll/Hep.

Under basal conditions, HK-2 cells on Coll/PEA or Coll/Levan showed comparable cell numbers as those on Coll (Fig. 6C). A trend for reduced cell numbers was observed after cell cultivation on Coll/sPEA. In contrast, HK-2 cells on Coll/sLevan or Coll/Hep displayed markedly higher numbers, reaching 2.0–3.5-fold and 2.5–3.7-fold the numbers compared to Coll, respectively. Under hyperglycemic conditions, HK-2 cells on Coll/PEA or Coll/Levan again remained close to Coll (Fig. 6D). Cells on Coll/sPEA were reduced by trend. HK-2 cell numbers on Coll/sLevan and Coll/Hep remained elevated, though less pronounced than under basal conditions, with 1.5–3.0-fold and 2.0–2.7-fold increases, respectively.

Immunofluorescence staining of HK-2 cells showed differences in cell density and morphology depending on the microenvironments (Fig. 6E and F). Under basal conditions (Fig. 6E), cells on Coll/PEA and Coll/Levan exhibited a spread morphology and cell coverage comparable to Coll. In contrast, cells on Coll/sPEA appeared sparse, consistent with the reduced metabolic activity. Coll/sLevan and Coll/Hep supported dense cell layers. Under hyperglycemic conditions, Coll/sLevan and Coll/Hep maintained higher cell coverage compared to Coll, whereas Coll/sPEA again showed reduced cell presence and cytoskeletal organization (Fig. 6F).

Additional experiments were performed to evaluate potential cytotoxic effects of the Coll/sLevan microenvironments on different cell types (SI Fig. S2B–D). No significant differences in metabolic activities were observed for HUVECs, pericytes, and HEK293 across the three coatings Coll, Coll/sLevan and Coll/Hep.

Sulfated levan-containing microenvironments suppress IL-6 release in renal epithelial cells

Given our previous observation that sLevan- and Hep-functionalized collagen matrices increase HK-2 cell numbers as a marker for enhanced proliferation, we quantified TGF-β1 and IL-6 secretion by ELISA to determine whether these biomimetic ECMs also modulate pro-fibrotic and pro-inflammatory mediator protein secretion (Fig. 7). Under basal conditions, latent TGF-β1 secretion was significantly elevated after HK-2 cultivation on Coll/Levan matrices compared to Coll, whereas no differences were observed between Coll and the other materials (Fig. 7A). Under hyperglycemic conditions, latent TGF-β1 levels were largely unchanged compared to Coll except for a significant reduction on Coll/sLevan and Coll/Hep (Fig. 7B). Latent TGF-β1 secretion on Coll itself was about 2.3-fold higher under hyperglycemic compared to basal conditions. Notably, active TGF-β1 remained below the ELISA detection limit under all conditions. Of note, HK-2 cells secreted significantly less latent TGF-β1 when cultured on collagen-based ECMs compared to TCPS surfaces under basal and hyperglycemic conditions.

IL-6 secretion differed across the material groups. Under basal conditions (Fig. 7C), HK-2 cells on Coll/Levan released approximately 2.3-fold higher IL-6 levels relative to Coll. In contrast, samples from Coll/sLevan contained reduced IL-6 levels (about 88% less than Coll). Under high glucose conditions (Fig. 7D), IL-6 secretion on Coll/Hep was reduced compared to Coll. IL-6 release from HK-2 cells on Coll/sPEA and Coll/sLevan remained low (88–94% less than Coll). No significant differences in IL-6 secretion were detected between cells cultured on TCPS and Coll. To exclude potential artefacts arising from IL-6 sequestration by the sulfated polysaccharides, we performed additional IL-6 binding assays with covalently immobilized polysaccharides, which revealed no significant interaction of sPEA starch, sLevan, or Hep with soluble IL-6 under physiological ionic strength (SI Fig. S3A). In addition, protein binding to the biomimetic microenvironments was assessed using rhodamine B-labeled lysozyme as a model GAG-binding protein (SI Fig. S3B). Compared to Coll, significantly reduced levels of unbound lysozyme were

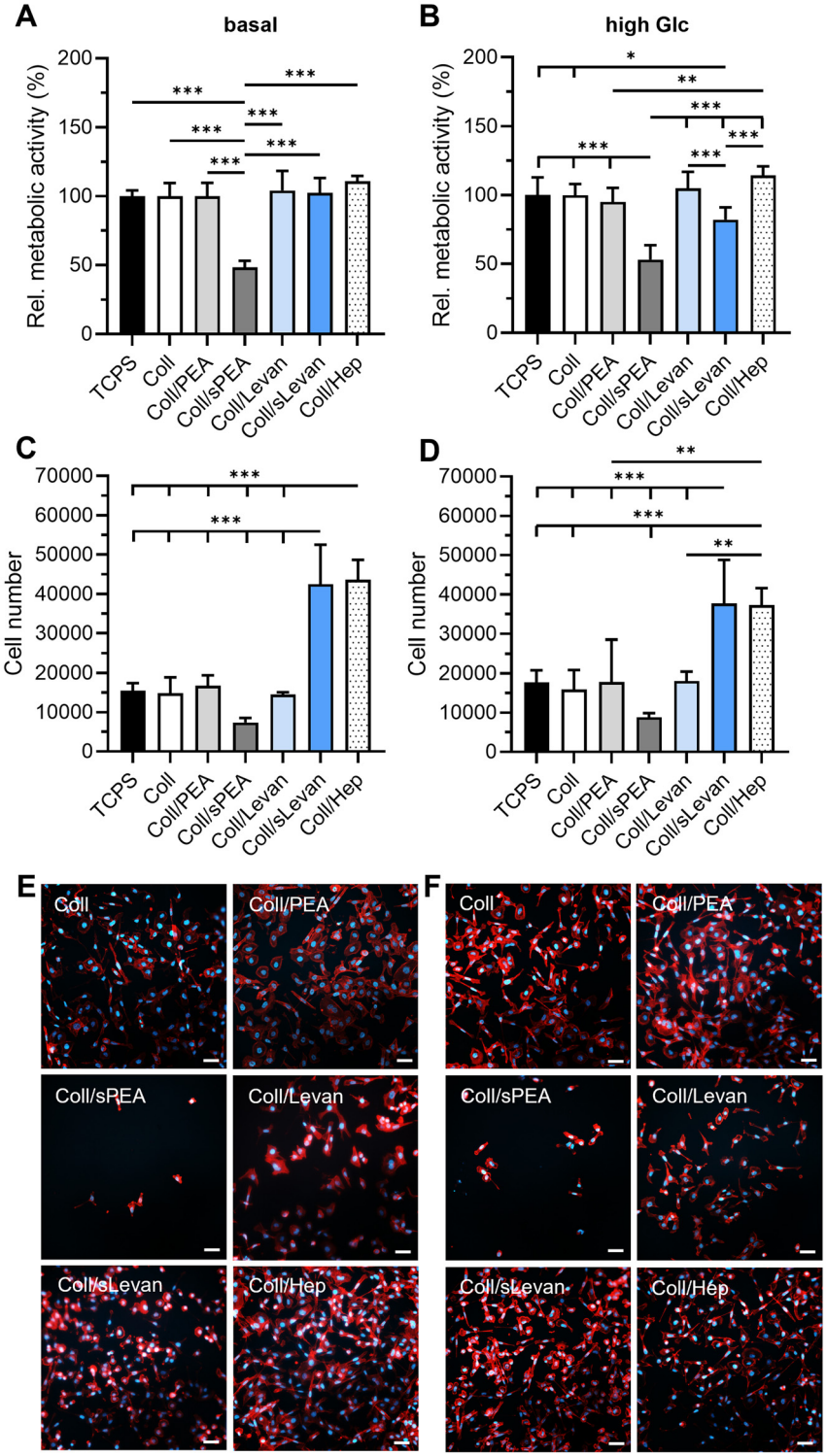

Fig. 6 Microenvironments containing sulfated levan promote HK-2 cell growth. HK-2 cells were cultured on microenvironments incorporating PEA starch, levan, and their sulfated derivatives. TCPS and Coll without polysaccharides served as controls and Hep-containing collagen coatings were included as reference. Cellular metabolic activity relative to cells on Coll (A and B) and DNA content (C and D) were quantified after 48 hours under basal conditions (A and C) or hyperglycemic conditions (B and D). Statistical analysis was performed using one-way ANOVA (*$p < 0.05$, **$p < 0.01$, ***$p < 0.001$). (E and F) Representative immunofluorescence images of HK-2 cells after 48 hours of culture on the coatings under basal medium (E) or hyperglycemic conditions (F). Nuclei were stained with DAPI (blue), and the actin cytoskeleton with phalloidin (red). Scale bar = 50 μm.

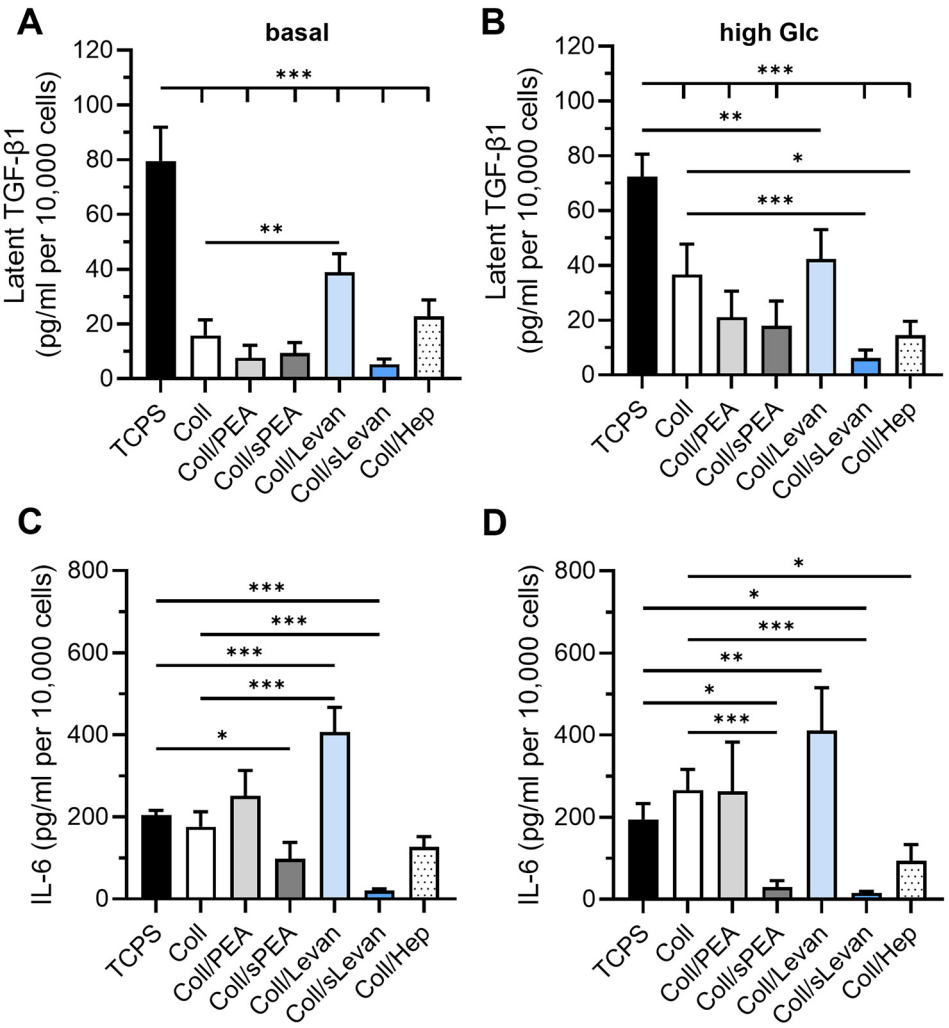

Fig. 7 Secretion of latent TGF-β1 and IL-6 by HK-2 cells cultured on self-assembled biomaterials. (A and B) latent TGF-β1 and (C and D) IL-6 secretion by HK-2 cells after 48 hours of culture on self-assembled materials containing PEA starch, levan, and their sulfated derivatives, compared to Hep-containing control materials. Panels (A) and (C) show cells cultured under basal conditions, whereas panels (B) and (D) correspond to high-glucose conditions. Protein levels quantified by ELISA were normalized to the measured cell numbers and are represented as fold-changes relative to the Coll control in basal media. TCPS and collagen-coated surfaces without GAGs or GAG mimetics served as references. One-way ANOVA: * $p < 0.05$, ** $p < 0.01$, *** $p < 0.001$. Significant differences relative to TCPS and Coll are indicated.

detected for Coll/Hep, Coll/sPEA, and Coll/sLevan, indicating increased protein binding. In contrast, Coll/PEA and Coll/Levan showed no significant differences compared to Coll (SI Fig. S3B). To assess osmotic effects, IL-6 secretion was analyzed in the presence of 30 mM mannitol and normalized to cell number (SI Fig. S4). While both glucose and mannitol increased IL-6 levels on Coll controls, sLevan-containing microenvironments consistently exhibited reduced IL-6 compared to Coll under all conditions.

Discussion

The present study explores sLevan and sPEA starch as non-animal-derived, polysaccharide-based GAG mimetics integrated into self-assembled collagen-based microenvironments, in which the structural matrix is derived from animal sources. Our aim was to engineer a functional coating capable of combining structural assembly with modulation of epithelial cell behavior. Previous publications highlighted the need for optimized materials as growth substrates for human tubular epithelial cells, since tissue-culture polystyrene, although not causing severe adverse effects on renal cell growth or survival, cannot recapitulate the complex composition, architecture, and regulatory functions of the native kidney ECM.[11,42,43] Developing well-defined, tunable ECM mimetics is particularly important for renal research, where epithelial repair, inflammation, and glucose-induced stress are tightly coordinated by cell–matrix interactions.

Chemical sulfation of both levan and PEA starch imparted anionic charge. NMR spectra confirmed substitution primarily at C1 in sLevan, with partial substitution at C3 and C4, consist-

ent with earlier analyses of sulfated polysaccharides.[25,44] The observed decrease in molar mass after sulfation is consistent with reports that sulfation reactions can partially depolymerize polysaccharides like hyaluronan (HA), which can influence bioactivity and release kinetics.[45–47] Polymer modifications by sulfation are known to enhance protein binding and mimic selected Hep functions, although anticoagulant potency remains lower due to the absence of the highly specific antithrombin-binding pentasaccharide sequence characteristic of Hep.[25,48–52] Likewise, sLevan and sPEA starch showed moderate anticoagulant activity (IC_{50} 5–6 μg mL^{-1} *vs.* 0.26 μg mL^{-1} for Hep), which is consistent with their structural features and indicates that polysaccharide sulfation confers some Hep-like interactions.

In this study, collagen type I was chosen as the structural ECM component since it is widely applied as an adhesion- and growth-promoting protein to improve mammalian cell culture and it is one of the main components of the kidney ECM.[11] Even though collagen type I is not part of the basal laminae, previous work studying the proliferation of HK-2 cells on different ECMs reported the highest cell numbers on collagen type I, type IV and gelatin, which were even higher than on laminin or Matrigel. Of note, the authors found a delay in cell growth on gelatin compared to the non-hydrolyzed collagen forms.[42]

During fibrillogenesis, individual collagen monomers spontaneously align and aggregate into fibrils when exposed to physiological conditions such as neutral pH, appropriate ionic strength, and temperature. These fibrils can further assemble into larger fibers, creating a scaffold that mimics the ECM. The presence of polysaccharides like GAGs can significantly influence this process.[28] GAGs are naturally occurring polysaccharides in the body that interact with collagen and other proteins in the ECM. When added to the *in vitro* fibrillogenesis process, GAGs can modulate the assembly of collagen fibrils by affecting factors such as fibril diameter, spacing, and the overall organization of the collagen network. Material stability analyses revealed that materials with sulfated polymers released more collagen and polysaccharide over time than those with non-sulfated counterparts. All microenvironments remained degradable by collagenase. Some differences occurred during early time points between the polymer-containing groups and Coll. Incorporation of polyanionic polymers likely increased hydration and loosened collagen fibril packing, as previously described for sulfated polymers, which may facilitate enzymatic access.[53,54]

The fibrillogenesis analysis demonstrated that sulfated polysaccharides strongly influence collagen fibrillogenesis in a concentration-dependent manner. At equimolar ratios, both sLevan and sPEA starch interfered with fibril formation, while at higher collagen-to-polysaccharide ratios normal sigmoidal kinetics reappeared. This effect likely arises from steric hindrance and electrostatic repulsion, consistent with reports that negatively charged polymers, such as dextran sulfate, iota-carrageenan or Hep, can alter the rate of fibrillogenesis affecting fibril formation and morphology.[55–58] This is further supported by our observation that non-sulfated levan shows reduced impact on fibrillogenesis at lower molecular weight, consistent with a contribution of steric hindrance at higher chain lengths. Accordingly, the observed effects cannot be attributed to sulfation alone but are likely to arise from a combination of charge density, molecular weight, and polymer structure. Interestingly, native PEA starch had little effect, highlighting that here sulfation rather than the carbohydrate backbone *per se* drives interference within collagen monomer association. Likewise, previous studies reported that the addition of highly sulfated GAG mimetics, like sulfated HA, concentration-dependently alters fibril formation leading to network-like structures with small microfibrils at 1/1 ratios with collagen.[28,36]

The biological assays underscored a functional divergence between sLevan and sPEA starch. In solution, sPEA starch induced a dose-dependent reduction in metabolic activity and cell number of HK-2 cells. On collagen coatings, Coll/sPEA starch similarly reduced proliferation and metabolic activity, consistent with an antiproliferative profile. In contrast, sLevan and Hep supported or even enhanced HK-2 proliferation, particularly under hyperglycemic conditions, while maintaining metabolic activity at levels comparable to collagen alone under basal conditions. Notably, discrepancies between metabolic activity and cell number, as observed for sLevan under high glucose conditions, suggest that metabolic readouts may not directly reflect cell viability but can also indicate shifts in cellular metabolic state induced by the microenvironment. The ability of sLevan to stimulate epithelial growth aligns with earlier observations that sLevan acts as a biocompatible Hep-mimetic for fibroblasts.[25] Likewise, soluble Hep was shown to reduce histone-mediated cytotoxicity in HK-2 cells.[59] This proliferative response is consistent with reports showing that higher GAG sulfation on collagen/HA or collagen/CS matrices induces a sulfate-dependent increase in dermal fibroblast proliferation.[60] In contrast, sulfated HA-based and over-sulfated CS as GAG mimetics induced a reduction of cell proliferation of rat osteoblasts and human keratinocytes,[41,61] underscoring both the importance of sulfation and the polysaccharide backbone for cell type-specific responses. However, no cytotoxic effects were observed after endothelial cell, pericyte and embryonic kidney cell culture on Coll/sLevan microenvironments, suggesting a wide cell compatibility of this material.

Kidney fibrosis is a central feature of chronic kidney disease progression, and HK-2 cells are known to secrete more pro-fibrotic TGF-β1 under hyperglycemic conditions,[62] which is consistent with our observations. Notably, latent TGF-β1 levels from HK-2 cells on Coll/sLevan and Coll/Hep under hyperglycemic conditions were reduced to values below those of Coll under basal conditions. To study the influence of polysaccharides associated with Coll on the modulation of inflammatory signaling in HK-2 cells, the IL-6 secretion was examined. IL-6 is described as a central mediator in diabetic kidney disease and tubular injury.[31,63] Furthermore, HK-2 are known to secrete IL-6 after stimulation.[64] For sPEA-containing microenvironments, reduced IL-6 levels likely reflect the markedly

decreased cell numbers and should not be interpreted as a specific anti-inflammatory effect. However, under both basal and high glucose conditions, Coll/sLevan suppressed IL-6 secretion from HK-2 cells, indicating an anti-inflammatory effect. Mechanistically, sLevan- and Hep-functionalized biomaterials might act as heparan sulfate mimetics that modulate the availability or activity of Hep-binding mitogens present in the cell culture media, such as acidic/basic fibroblast growth factors, insulin-like growth factor (IGF)-1 in complex with IGF-binding proteins, and Hep-binding epidermal growth factor-like growth factors.[65–68] Previous studies showed that IGF-1 can suppress IL-6 expression and exert anti-inflammatory effects in several peripheral tissues, whereas EGF/EGFR signaling in the kidneys promotes tubular repair rather than sustaining pro-inflammatory responses.[69,70] Adsorbed protein layers are widely recognized as key mediators between biomaterial surface chemistry and integrin-dependent cellular responses.[71,72] Additional lysozyme binding experiments demonstrated material-dependent differences in protein/matrix interactions, supporting an indirect mechanism *via* modulation of protein availability and cell/matrix signaling. The inclusion of an osmotic control showed that both glucose and mannitol contribute to IL-6 regulation. However, the persistent reduction of IL-6 on sLevan coatings under all conditions indicates a material-specific modulation of epithelial cell responses that cannot be explained by osmotic effects alone.

Taken together, the data support a model in which polysaccharide sulfation alters both material assembly and cellular responses. Importantly, the divergent effects of sLevan and sPEA within the same collagen platform indicate that sulfation alone is insufficient to predict epithelial responses, highlighting polysaccharide backbone-dependent modulation of collagen organization and cell behavior. While sPEA starch exerts antiproliferative and potentially cytotoxic effects, sLevan combines moderate anticoagulant activity with enhanced epithelial proliferation and suppression of pro-fibrotic and inflammatory protein release, even under hyperglycemic stress. By extending previous non-renal applications of sLevan and related sulfated polysaccharide-based biomaterials to a kidney epithelial setting, these findings position Coll/sLevan as a promising candidate for renal biomaterial coatings where promotion of epithelial repair and reduction of glucose-induced inflammation are desirable.

However, we acknowledge potential limitations of our study. The HK-2 cell line, although immortalized, represents a simplified model of human proximal tubule epithelium. While it does not fully reproduce the heterogeneity and donor-specific variability of primary human cells,[73] it remains a well-established and accepted model system that retains key transport, metabolic, and inflammatory signaling pathways and offers the experimental reproducibility necessary for mechanistic investigations where primary cells are scarce and variable.[74] Similarly, the high-glucose conditions used here exceed physiological plasma concentrations. Nevertheless, the used concentration is a well-established *in vitro* paradigm for inducing high-glucose-mediated stress in proximal tubule cells and has been extensively validated to reproducibly activate oxidative, inflammatory, and pro-fibrotic responses characteristic of diabetic kidney injury. For example, previous studies have shown that it reliably induces apoptosis and stress signaling in HK-2 cells compared with normoglycemic controls.[75] Future *in vivo* studies will be required to evaluate immunogenicity, long-term stability, and functional integration of these materials within the renal microenvironment. Despite these limitations, our results demonstrate that sLevan derivatives provide bioactive, ECM-mimetic substrates capable of modulating epithelial cell activity and secretory responses, underscoring their relevance and translational potential for renal tissue engineering and disease modeling.

Conclusion

In conclusion, we demonstrate that self-assembled collagen/sLevan microenvironments provide a well-defined structural matrix that is enzymatically degradable, exhibits moderate anticoagulant activity, and supports favorable epithelial responses, including enhanced proliferation and reduced IL-6 and TGF-β1 secretion under hyperglycemic conditions. These combined properties underscore their potential as sustainable, non-animal-derived GAG-mimetic components within collagen-based biomaterial systems for regenerative applications, particularly in renal tissue engineering under hyperglycemic or inflammatory conditions.

Author contributions

Dunya Arabi: data curation, formal analysis, investigation, writing – review and editing. Annika Clemenz: data curation, formal analysis, investigation, writing – review and editing. Cedric Wilden: data curation, formal analysis, investigation, writing – original draft. Paula Marie Schindler: data curation, formal analysis, investigation, writing – review and editing. Julia Decker: data curation, formal analysis, investigation, writing – review and editing. Nsrin Aroub: data curation, formal analysis, investigation, writing – review and editing. Albrecht Berg: data curation, formal analysis, investigation, writing – original draft. Wolfgang Metzger: data curation, formal analysis, investigation, writing – review and editing. Maike Derenek: data curation, formal analysis, investigation, writing – review and editing. Samer Alokaidi: data curation, formal analysis, investigation, writing – review and editing. Karin Jacobs: methodology, resources, writing – review and editing. Philipp Jung: methodology, resources, writing – review and editing. Matthias W. Laschke: conceptualization, methodology, resources, writing – review and editing. Emmanuel Ampofo: conceptualization, methodology, resources, writing – review and editing. Sandra Rother: conceptualization, investigation, data curation, methodology, funding acquisition supervision, project administration, writing – original draft.

Conflicts of interest

There are no conflicts to declare.

Data availability

The authors confirm that the data supporting the findings of this study are available within the article and its supplementary information (SI). Supplementary information: fibrillogenesis kinetics in the presence of levan (5 kDa); DNA per cell values of HK-2 cells; metabolic activity of HUVEC, pericytes and HEK-293 cells on Coll, Coll/sLevan and Coll/Hep; binding of human IL-6 to covalently immobilized sPEA, sLevan or Hep; binding of rhodamine B-labeled lysozyme to coatings; IL-6 secretion of HK-2 cells under osmotic and hyperglycemic conditions. See DOI: https://doi.org/10.1039/d5bm01849h.

Acknowledgements

We would like to thank Daniela Sossong for her technical support during cell cultivation. This research was financially supported by Dr Rolf M. Schwiete Stiftung, grant number 2024-021. K. J. and P. J. acknowledge support by the German Research Foundation (DFG) large instrument funding under grant numbers INST 256/542-1 FUGG (project number 449375068) and INST 256/583-1 FUGG (project number 519828155). S. A. and K. J. thank the DFG priority program SPP 2451 "Engineered Living Materials with Adaptive Functions" for funding (project number 541302782). M. D. is supported by the DFG priority program 2332 (project 1).

References

1 K. J. Jager, C. Kovesdy, R. Langham, M. Rosenberg, V. Jha and C. Zoccali, *Nephrol., Dial., Transplant.*, 2019, **34**, 1803–1805.
2 J. C. Lv and L. X. Zhang, *Adv. Exp. Med. Biol.*, 2019, **1165**, 3–15.
3 C. P. Kovesdy, *Kidney Int. Suppl.*, 2022, **12**, 7–11.
4 K. L. Lentine, J. M. Smith, J. M. Miller, K. Bradbrook, L. Larkin, S. Weiss, D. K. Handarova, K. Temple, A. K. Israni and J. J. Snyder, *Am. J. Transplant.*, 2023, **23**, S21–S120.
5 D. A. Papazova, N. R. Oosterhuis, H. Gremmels, A. Van Koppen, J. A. Joles and M. C. Verhaar, *Dis. Models Mech.*, 2015, **8**, 281–293.
6 K. Tajima, H. Yagi, T. Morisaku, K. Nishi, H. Kushige, H. Kojima, H. Higashi, K. Kuroda, M. Kitago, S. Adachi, T. Natsume, K. Nishimura, M. Oya and Y. Kitagawa, *NPJ Regen. Med.*, 2022, **7**, 1–12.
7 R. Sobreiro-Almeida, R. Quinteira and N. M. Neves, *Adv. Healthcare Mater.*, 2021, **10**, 2100160.
8 R. Quinteira, S. Gimondi, N. O. Monteiro, R. Sobreiro-Almeida, L. Lasagni, P. Romagnani and N. M. Neves, *Acta Biomater.*, 2024, **180**, 295–307.
9 A. Naba, *Nat. Rev. Mol. Cell Biol.*, 2024, **25**, 865–885.
10 K. Gelse, E. Pöschl and T. Aigner, *Adv. Drug Delivery Rev.*, 2003, **55**, 1531–1546.
11 A. Lacueva-Aparicio, R. S. Lindoso, S. M. Mihăilă and I. Giménez, *Front. Physiol.*, 2022, **13**, 1048738.
12 J. Su, S. C. Satchell, R. N. Shah and J. A. Wertheim, *J. Biomed. Mater. Res., Part A*, 2018, **106**, 2448–2462.
13 R. Quinteira, S. Gimondi, N. O. Monteiro, R. Sobreiro-Almeida, L. Lasagni, P. Romagnani and N. M. Neves, *Acta Biomater.*, 2024, **180**, 295–307.
14 D. E. Soranno, C. B. Rodell, C. Altmann, J. Duplantis, A. Andres-Hernando, J. A. Burdick and S. Faubel, *Am. J. Physiol.: Renal Physiol.*, 2016, **311**, F362–F372.
15 R. V. Iozzo and L. Schaefer, *Matrix Biol.*, 2015, **42**, 11–55.
16 L. Schaefer and R. M. Schaefer, *Cell Tissue Res.*, 2010, **339**, 237–246.
17 A. Badri, A. Williams, R. J. Linhardt and M. A. Koffas, *Curr. Opin. Biotechnol.*, 2018, **53**, 85–92.
18 Q. Liu, G. Chen and H. Chen, *Polym. Chem.*, 2018, **10**, 164–171.
19 D. Scharnweber, L. Hübner, S. Rother, U. Hempel, U. Anderegg, S. A. Samsonov, M. T. Pisabarro, L. Hofbauer, M. Schnabelrauch, S. Franz, J. Simon and V. Hintze, *J. Mater. Sci. Mater. Med.*, 2015, **26**, 232.
20 E. T. Öner, L. Hernández and J. Combie, *Biotechnol. Adv.*, 2016, **34**, 827–844.
21 E. Raga-Carbajal, A. Diaz-Vilchis, S. Rojas-Trejo, E. Rudino-Pinera and C. Olvera, *J. Biol. Chem.*, 2021, **296**, 100178.
22 B. Y. Byun, S. J. Lee and J. H. Mah, *Int. J. Food Sci. Technol.*, 2014, **49**, 238–245.
23 A. D. Sedgwick, A. Rutman, Y. M. Sin, A. R. Mackay and D. A. Willoughby, *Br. J. Exp. Pathol.*, 1984, **65**, 215.
24 W. M. Muriel and S. Karboune, *Food Chem.*, 2025, **494**, 145981.
25 M. Erginer, A. Akcay, B. Coskunkan, T. Morova, D. Rende, S. Bucak, N. Baysal, R. Ozisik, M. S. Eroglu, M. Agirbasli and E. Toksoy Oner, *Carbohydr. Polym.*, 2016, **149**, 289–296.
26 T. D. Gomes, S. G. Caridade, M. P. Sousa, S. Azevedo, M. Y. Kandur, E. T. Öner, N. M. Alves and J. F. Mano, *Acta Biomater.*, 2018, **69**, 183–195.
27 T. Douglas, S. Heinemann, S. Bierbaum, D. Scharnweber and H. Worch, *Biomacromolecules*, 2006, **7**, 2388–2393.
28 A. Miron, S. Rother, L. Huebner, U. Hempel, I. Käppler, S. Moeller, M. Schnabelrauch, D. Scharnweber, V. Hintze, K. Iris, S. Moeller, M. Schnabelrauch, D. Scharnweber and V. Hintze, *Macromol. Biosci.*, 2014, **14**, 1783–1794.
29 M. Cortes-Medina, A. R. Bushman, P. E. Beshay, J. J. Adorno, M. M. Menyhert, R. M. Hildebrand, S. S. Agarwal, A. Avendano, A. K. Friedman and J. W. Song, *Acta Biomater.*, 2024, **174**, 116–126.
30 J. M. Muñoz-Félix, M. González-Núñez, C. Martínez-Salgado and J. M. López-Novoa, *Pharmacol. Ther.*, 2015, **156**, 44–58.

31 L. Zhang, F. Xu and L. Hou, *Front. Immunol.*, 2024, **15**, 1465625.
32 X. B. Yang, X. D. Gao, F. Han and R. X. Tan, *Biochim. Biophys. Acta*, 2005, **1725**, 120–127.
33 S. Geresh, A. Mamontov and J. Weinstein, *J. Biochem. Biophys. Methods*, 2002, **50**, 179–187.
34 X. Nie, B. Shi, Y. Ding and W. Tao, *Int. J. Biol. Macromol.*, 2006, **39**, 228–233.
35 T. Douglas, U. Hempel, C. Mietrach, M. Viola, D. Vigetti, S. Heinemann, S. Bierbaum, D. Scharnweber and H. Worch, *J. Biomed. Mater. Res., Part A*, 2008, **84A**, 805–816.
36 S. Rother, J. Salbach-Hirsch, S. Moeller, T. Seemann, M. Schnabelrauch, L. C. Hofbauer, V. Hintze and D. Scharnweber, *ACS Appl. Mater. Interfaces*, 2015, **7**, 23787–23797.
37 R. W. Farndale, D. J. Buttle and A. J. Barrett, *Biochim. Biophys. Acta*, 1986, **883**, 173–177.
38 A. K. Picke, J. Salbach-Hirsch, V. Hintze, S. Rother, M. Rauner, C. Kascholke, S. Möller, R. Bernhardt, S. Rammelt, M. T. Pisabarro, G. Ruiz-Gómez, M. Schnabelrauch, M. Schulz-Siegmund, M. C. Hacker, D. Scharnweber, C. Hofbauer and L. C. Hofbauer, *Biomaterials*, 2016, **96**, 11–23.
39 F. H. Silver and D. E. Birk, *Collagen Relat. Res.*, 1983, **3**, 393–405.
40 V. Hintze, A. Miron, S. Moeller, M. Schnabelrauch, H. P. Wiesmann, H. Worch and D. Scharnweber, *Acta Biomater.*, 2012, **8**, 2144–2152.
41 L. Corsuto, S. Rother, L. Koehler, E. Bedini, S. Moeller, M. Schnabelrauch, V. Hintze, C. Schiraldi and D. Scharnweber, *Carbohydr. Polym.*, 2018, **191**, 53–64.
42 H. Zhang, F. Tasnim, J. Y. Ying and D. Zink, *Biomaterials*, 2009, **30**, 2899–2911.
43 R. C. Van Gaal, A. F. Vrehen, J. F. Van Sprang, P. P. K. H. Fransen, M. C. Van Turnhout and P. Y. W. Dankers, *Biomater. Sci.*, 2021, **9**, 2209–2220.
44 J. Kärkkäinen, T. R. Wik, M. Niemelä, K. Lappalainen, P. Joensuu and M. Lajunen, *Carbohydr. Polym.*, 2016, **136**, 721–727.
45 V. Hintze, M. Schnabelrauch and S. Rother, *Front. Chem.*, 2022, **10**, 830671.
46 Q. Chen, M. Zhang, Y. Liu, W. Liu, C. Peng and L. Zheng, *Chem. Biodivers.*, 2024, **21**, e202400152.
47 V. Hintze, S. Moeller, M. Schnabelrauch, S. Bierbaum, M. Viola, H. Worch and D. Scharnweber, *Biomacromolecules*, 2009, **10**, 3290–3297.
48 M. W. Olson, *J. Biol. Chem.*, 1997, **272**, 29975–29983.
49 A. Magnani, S. Lamponi, R. Rappuoli and R. Barbucci, *Polym. Int.*, 1998, **46**, 225–240.
50 N. M. Mestechkina and V. D. Shcherbukhin, *Appl. Biochem. Microbiol.*, 2010, **46**, 267–273.
51 B. Casu, P. Oreste, G. Torri, G. Zoppetti, J. Choay, J. C. Lormeau, M. Petitou and P. Sinäy, *Biochem. J.*, 1981, **197**, 599–609.
52 F. Depasse, G. T. Gerotziafaz, J. Busson, P. Van Dreden and M. M. Samama, *J. Thromb. Haemostasis*, 2004, **2**, 346–348.
53 P. Riedl, M. Schricker and T. Pompe, *Gels*, 2021, **7**, 266.
54 H. W. Ng, Y. Zhang, R. Naffa and S. Prabakar, *Gels*, 2020, **6**, 1–11.
55 J. M. Mcpherson, S. J. Sawamura, R. A. Condell, W. Rhee and D. G. Wallace, *Collagen Relat. Res.*, 1988, **8**, 65–82.
56 D. Stamov, M. Grimmer, K. Salchert, T. Pompe and C. Werner, *Biomaterials*, 2008, **29**, 1–14.
57 K. Stuart and A. Panitch, *Biopolymers*, 2008, **89**, 841–851.
58 T. E. Robinson, M. Y. Brunet, I. Chapple, A. H. M. Heagerty, A. D. Metcalfe and L. M. Grover, *Adv. NanoBiomed Res.*, 2023, **3**, 2300048.
59 Z. Wang, L. Wang, C. Cao, H. Jin, Y. Zhang, Y. Liu, Y. Gao, X. Liang, G. Li and S. Shou, *Front. Med.*, 2020, **7**, 586652.
60 A. van der Smissen, V. Hintze, D. Scharnweber, S. Moeller, M. Schnabelrauch, A. Majok, J. C. Simon and U. Anderegg, *Biomaterials*, 2011, **32**, 8938–8946.
61 R. Kunze, M. Rösler, S. Möller, M. Schnabelrauch, T. Riemer, U. Hempel and P. Dieter, *Glycoconjugate J.*, 2010, **27**, 151–158.
62 C. E. Hills, E. Siamantouras, S. W. Smith, P. Cockwell, K. K. Liu and P. E. Squires, *Diabetologia*, 2012, **55**, 812–824.
63 F. F. Kreiner, J. M. Kraaijenhof, M. von Herrath, G. K. K. Hovingh and B. J. von Scholten, *Expert Rev. Clin. Immunol.*, 2022, **18**, 377–389.
64 M. Y. Huang, L. S. Chaturvedi, S. Koul and H. K. Koul, *Kidney Int.*, 2005, **68**, 497–503.
65 P. L. Ho, E. Caron, H. A. Armelin and A. G. Gambarini, *Braz. J. Med. Biol. Res.*, 1988, **21**, 203–212.
66 M. A. Nugent and R. V. Iozzo, *Int. J. Biochem. Cell Biol.*, 2000, **32**, 115–120.
67 T. Arai, W. Busby and D. R. Clemmons, *Endocrinology*, 1996, **137**, 4571–4575.
68 D. T. Dao, L. Anez-Bustillos, R. M. Adam, M. Puder and D. R. Bielenberg, *Am. J. Pathol.*, 2018, **188**, 2446.
69 S. Rayego-Mateos, R. Rodrigues-Diez, J. L. Morgado-Pascual, F. Valentijn, J. M. Valdivielso, R. Goldschmeding and M. Ruiz-Ortega, *Mediators Inflamm.*, 2018, **2018**, 8739473.
70 M. Spies, O. Nesic, R. E. Barrow, J. R. Perez-Polo and D. N. Herndon, *Gene Ther.*, 2001, **8**, 1409–1415.
71 C. J. Wilson, R. E. Clegg, D. I. Leavesley and M. J. Pearcy, *Tissue Eng.*, 2005, **11**, 1–18.
72 B. G. Keselowsky, D. M. Collard and A. J. García, *J. Biomed. Mater. Res., Part A*, 2003, **66**, 247–259.
73 S. E. Jenkinson, G. W. Chung, E. van Loon, N. S. Bakar, A. M. Dalzell and C. D. A. Brown, *Pflugers Arch.*, 2012, **464**, 601–611.
74 M. J. Ryan, G. Johnson, J. Kirk, S. M. Fuerstenberg, R. A. Zager and B. Torok-Storb, *Kidney Int.*, 1994, **45**, 48–57.
75 X. Q. Zhang, J. J. Dong, T. Cai, X. Shen, X. J. Zhou and L. Liao, *Oncotarget*, 2017, **8**, 24119–24129.